

## Jet Deflection by Very Weak Guide Fields during Magnetic Reconnection

M. V. Goldman,<sup>1</sup> G. Lapenta,<sup>2</sup> D. L. Newman,<sup>1</sup> S. Markidis,<sup>2</sup> and H. Che<sup>1</sup>

<sup>1</sup>*Department of Physics and CIPS, University of Colorado, Boulder, Colorado 80309, USA*

<sup>2</sup>*Centrum voor Plasma-Astrofysica, Katholieke Universiteit, Leuven, Belgium*

(Received 16 July 2010; published 19 September 2011)

Previous 2D simulations of reconnection using a standard model of initially antiparallel magnetic fields have detected electron jets outflowing from the  $x$  point into the ion outflow exhausts. Associated with these jets are extended “outer electron diffusion regions.” New PIC simulations with an ion to electron mass ratio as large as 1836 (an  $H^+$  plasma) now show that the jets are strongly deflected and the outer electron diffusion region is broken up by a very weak out-of-plane magnetic guide field, even though the diffusion rate itself is unchanged. Jet outflow and deflection are interpreted in terms of electron dynamics and are compared to recent measurements of jets in the presence of a small guide field in Earth’s magnetosheath.

DOI: 10.1103/PhysRevLett.107.135001

PACS numbers: 52.35.Vd, 52.20.Dq, 52.65.Rr, 94.30.cp

Magnetic reconnection is currently one of the most actively studied processes in plasma physics. It is believed to be responsible for solar flares, coronal mass ejections, and magnetospheric substorms. The study of *electron-scale* processes associated with magnetic reconnection in the magnetosphere is one of NASA’s highest priorities—to culminate in 2014 with the launch of the Multiscale Magnetosphere Satellites that will be able to resolve electron features of reconnection up to 100 times faster than existing satellites.

Many particle-in-cell (PIC) simulation [1–3] studies of electron-scale physics during reconnection employ a common (standard) model of 2D *antiparallel* reconnection in which the initial magnetic field,  $\mathbf{B} = \hat{\mathbf{x}}B_0 \tanh(y/\Delta y)$ , lies entirely in a plane (here taken as the  $x$ - $y$  plane), as in early MHD simulations. There are many predictions from such standard PIC simulations which are often taken as essential signatures of reconnection—symmetric Hall currents and fields, symmetric particle densities, and particle outflow centered in the exhausts. Such outflow includes electron jets, coherently directed and extended deep into the exhausts (“ $x$ ” direction), accompanied by elongated “outer diffusion regions.”

However, just as with 2D MHD simulations [4], it is now becoming evident that these features are dramatically changed by even small departures from the assumptions of the standard model. In particular, the addition of a guide field,  $B_g$ , much smaller than the asymptotic reconnecting field,  $B_0$ , can have profound effects [5].

In this Letter, we provide evidence from PIC reconnection simulations [6] (with an ion-to-electron mass ratio of up to  $M/m = 1836$ ) that guide fields of  $B_g = 0.05B_0$  and  $0.1B_0$  are sufficient to deflect and distort the jets from the  $x$  axis towards separatrix legs, while the reconnection rate remains essentially unchanged.

Cluster measurements [7] reported in Physical Review Letters during symmetric magnetosheath reconnection have

been interpreted as evidence for an elongated narrow jet in  $v_{ex}$  of width  $9d_e = 9c/\omega_{pe} = 11$  km (Fig. 1). Asymptotic reversing  $B_x$  fields of  $B_0 = \pm 40$  nT were measured both at the exhaust entry and exit. A guide field of  $B_g = 7$  nT was measured at the exhaust entry *and* at the inferred jet location itself [Fig. 1(a)]. Hence,  $B_g = 0.16B_0$  to good accuracy. Such jets would be consistent with outer diffusion regions similar to those found in explicit PIC simulations [1,2] with *no* guide field and ion-to-electron mass ratio  $M/m = 25$ . The new reconnection simulations in this Letter *do show* jet deflection using  $M/m$  as high as 1836 and guide fields,  $B_g$ , *smaller than the measured*  $B_g = 0.16B_0$ . This disagreement will be addressed in the conclusion.

In order to determine how electron jets depend on the guide field, new implicit [6] 2D PIC simulations of spontaneous reconnection have been performed. The initial state is a perturbed Harris equilibrium, with  $B_x(y) = B_0 \tanh(y/\Delta y)$ , where  $\Delta y$  is the initial current sheet thickness, taken here to be  $d_i/2$ . Initial electron and ion temperatures are  $T_{e0}/m_e c^2 = (v_{eth0}/c)^2 = 2 \times 10^{-3}$ , and  $T_{i0} = 5T_{e0}$ . The background density is  $n_b = 0.1n_0$ , where  $n_0$  is the peak initial density.

In Fig. 2(a),  $v_{ex}(x, y)/v_{eth0}$ , the dominant component of the electron flow velocity,  $\mathbf{v}_e/v_{eth0}$ , is compared at the same time,  $\Omega_i t = 14.2$ , in three reconnection simulations for  $M/m = 1836$  and various  $\mathbf{B}_g$ . Note the expanded aspect ratio of  $y$  to  $x$ .

For  $B_g = 0$  [Fig. 2(a)], incipient outgoing collimated jets flow out from the  $x$  point along the  $\pm x$  axis at  $y = 10d_i$ . However, even for  $B_g = 0.05B_0$ , [Fig. 2(b)], the jets are split and deflected. For  $B_g = 0.1B_0$  [Fig. 2(c)] the deflection of jets by the Lorentz force associated with  $B_g$  has resulted in dominant beams elongated along appropriate separatrix legs.

The net electric plus magnetic force [1,2,8,9] is  $\mathbf{F}(x, y) = -e\mathcal{E}(x, y)$ , where  $\mathcal{E}$  is defined as a generalized “field,”

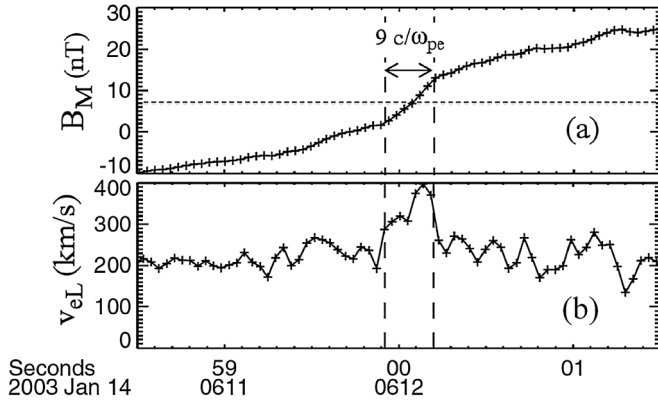


FIG. 1. (a): Measured  $B_M = B_z$  with  $B_g = 7$  nT (dashed horizontal line). (b) Inferred jet in  $v_{eL} = v_{ex}$ . (Adapted with permission from Ref [7]).

$\mathcal{E} = \mathbf{E} + (\mathbf{v} \times \mathbf{B})/c$ . In Fig. 3, components of  $\mathcal{E}(x, y)$  are plotted at the same time,  $t\Omega_i = 14.2$ , as in Fig. 2. For  $B_g = 0$  [Fig. 3(a)], the inflowing electron  $y$  velocity,  $v_{ey}(x, y)$  is essentially frozen-in ( $= cE_z/B_x$ ) just above and below the central (blue [dark gray]) “inner” diffusion region. The flanking (red [medium gray]) regions are the early “outer” diffusion regions [1,2].

For the case  $B_g = 0.1B_0$ , [Fig. 3(b)] the inner diffusion region is distorted, but more significantly, the outer diffusion region is no longer elongated in  $x$  or collimated in  $y$ . The reconnection rate, however, is not significantly changed.

Figures 3(c) and 3(d) show  $\mathcal{E}_x$  and  $\mathcal{E}_y$ , respectively, for  $B_g = 0$ . The yellow rectangles enclose regions where, to a good approximation,  $\mathcal{E}_x \propto -x$  and  $\mathcal{E}_y \propto y$ . The  $y$  boundaries of this region are the  $y$  boundaries of the jets [Fig. 1(a)] (same as the  $y$  boundaries of the *current sheet*). The boundaries at  $x = \pm 0.4d_i$  are at about half the values of the  $x$  boundaries of the jets. The force,  $-e\mathcal{E}_x \propto x$ , accelerates electrons away from the  $x$  point at  $x = 20d_i$  to form the

outgoing jets. The dominant contribution to  $-e\mathcal{E}_x$  in this region is the Lorentz force,  $ev_{ez}B_y(x)/c$ , due to the out-of-plane almost-uniform velocity  $v_{ez}$  of the electron *current sheet* and the in-plane  $B_y(x)$  of the *reconnected* field lines [1,2].  $E_x$  is about half as large as  $v_{ez}B_y(x)/c$  inside this region but dominates outside where it can cause oscillations (trapping) in  $x$  in both the inflow region and the exhaust [2,9].

In Fig. 3(d),  $-e\mathcal{E}_y(y) \propto -y$  is a *restoring* force in  $y$  inside the yellow box. It *traps the jet in the y direction* and keeps it from expanding in  $y$ . Once again, the *Lorentz* force,  $ev_{ez}B_x(y)/c$  contribution is about twice as big as the (*Hall*) *electric field* force,  $-eE_y$ .

The dynamical equations for the 2D motion of an electron due to in-plane fields  $E_{x,y}(x, y)$  and  $B_{x,y}(x, y)$  underlying Figs. 3(c) and 3(d), together with the Lorentz force of a weak guide field,  $B_g \leq 0.1B_0$  are

$$\ddot{x} + \frac{e}{m} \left[ E_x(x, y) - \frac{\dot{z}B_y(x, y)}{c} \right] = -\Omega_{eg}\dot{y}, \quad (1a)$$

$$\ddot{y} + \frac{e}{m} \left[ E_y(x, y) + \frac{\dot{z}B_x(x, y)}{c} \right] = \Omega_{eg}\dot{x}. \quad (1b)$$

Here,  $\Omega_{eg} = eB_g/m_e c$ . Assume now that  $\dot{z}$  is equal to its initial value,  $\dot{z}_0$ , which, in turn, is set equal to  $v_{ez}$  of the current sheet in the linear region, where it is essentially independent of  $x$  and  $y$ . Neglect of the dynamical evolution of  $\dot{z}$  away from its initial value,  $\dot{z}_0$  has been verified numerically and sets this treatment apart from that of the so-called Speiser orbits [10]. For  $B_g = 0$  the square brackets in Eqs. (1) can be approximated as  $\mathcal{E}_x(x) \propto -x$  and  $\mathcal{E}_y(y) \propto y$  in the yellow boxes in Figs. 3(c) and 3(d). They remain approximately stationary and equal to their values at time 14.2 throughout the electron motion. The equations of motion in the linear region are

$$\ddot{x} - \gamma_x^2 x \approx -\Omega_{eg}\dot{y}, \quad \ddot{y} + \omega_y^2 y \approx \Omega_{eg}\dot{x}. \quad (2)$$

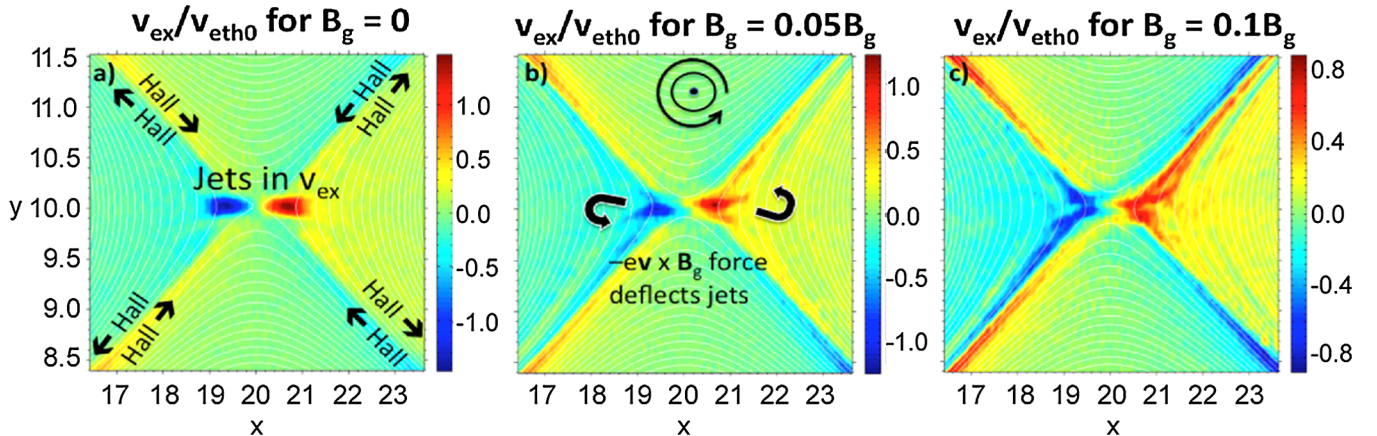


FIG. 2 (color online). Deflection of jet in the  $x$  velocity of electrons,  $v_{ex}/v_{eth0}$ , by small guide fields ( $M/m = 1836$ ). (a)  $B_g = 0$ ; (b)  $B_g/B_0 = 0.05$ ; (c)  $B_g/B_0 = 0.1$ .  $x$  and  $y$  in units of  $d_i$ . Note expanded aspect ratio.

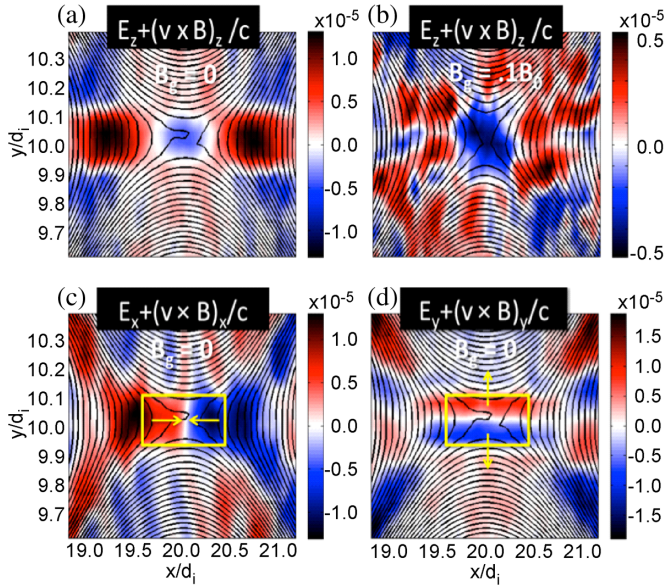


FIG. 3 (color online). Components of electric-magnetic force “field,”  $\mathcal{E} = -\mathbf{F}/e = \mathbf{E} + (\mathbf{v} \times \mathbf{B})/c$  in simulation units,  $\sqrt{4\pi n_0 m_i c^2}$  ( $M/m = 1836$ ,  $t\Omega_i = 14.2$ ). (a)  $\mathcal{E}_z$  for  $B_g = 0$ ; (b) Same for  $B_g = 0.1 B_0$ , (c)  $\mathcal{E}_x$  and (d)  $\mathcal{E}_y$ , for  $B_g = 0$ . Yellow arrows show direction of  $\mathcal{E}_x$  and  $\mathcal{E}_y$ . Rectangles enclose “linear” regions.

The linear coefficients are  $\gamma_x^2 \equiv -\omega_e^2 [\partial_{x'} \mathcal{E}_x^{\text{sim}}(x')]_{x'=0} > 0$  and  $\omega_y^2 \equiv \omega_e^2 [\partial_{y'} \mathcal{E}_y^{\text{sim}}(y')]_{y'=0} > 0$ . The zeros of  $x$  and  $y$  have been relocated to the  $x$  point. Distances are in ion inertial lengths,  $d_i$ . From Figs. 3(c) and 3(d), the rates are roughly  $\gamma_x/\Omega_{e0} = 0.035$  and  $\omega_y/\Omega_{e0} = 0.066$ , where  $\Omega_{e0}$  is the electron cyclotron frequency in  $B_0$ .

The initial position of a characteristic [11] trajectory is chosen as  $x_0 = 0$  and  $y_0 = 0.09d_i$ . The initial  $y$ -drift velocity at  $y_0$  is taken from the simulation to be  $\dot{y}_0 = -0.2v_{\text{eth0}}$ . A small initial velocity,  $\dot{x}_0 = 0.2v_{\text{eth0}}$  is chosen, consistent with  $E_x$ . At  $\{x_0, y_0\}$  the downward moving electron begins to feel the  $y$  force, which eventually turns it back up again in  $y$  as it is accelerated in  $x$ . When  $B_g = 0$ ,  $x(t) \propto \sinh(\gamma_x t)$  and  $y(t) \propto \cos(\omega_y t)$ . For  $B_g = 0.1B_0$ , both  $x$  and  $y$  are linear combinations of  $\sinh(\gamma' t)$ ,  $\cosh(\gamma' t)$ ,  $\sin(\omega' t)$  and

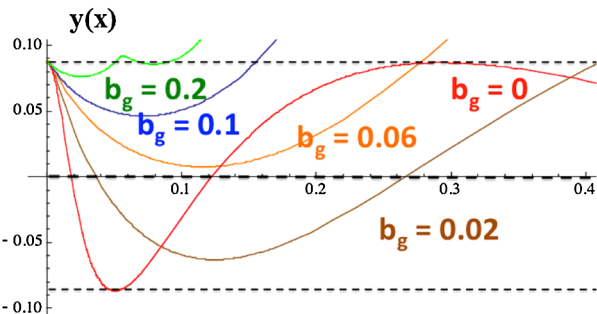


FIG. 4 (color online). Parametric plots of  $y(x)$  solutions to Eqs. (2) for  $b_g = B_g/B_0 = 0, 0.02, 0.06, 0.1, 0.2$ .  $M/m = 1836$ .

$\cos(\omega' t)$ , so that  $y$  is now growing as well as oscillating. Here,  $\omega'$  and  $\gamma'$  are solutions to the eigenvalue equation for the linear Eqs. (2):  $2\{\omega'^2, -\gamma'^2\} = [\Omega_{eg}^2 + (\omega_y^2 - \gamma_x^2)] \pm \sqrt{4\omega_y^2 \gamma_x^2 + [\Omega_{eg}^2 + (\omega_y^2 - \gamma_x^2)]^2}$ . In Fig. 4 the parametric trajectories  $y(x)$  are plotted for  $B_g/B_0 = 0, 0.02, 0.06, 0.1$  and  $0.2$ . For  $B_g = 0$ , the trajectory is bounded in  $y$  and extends out in  $x$ . For  $B_g \neq 0$  the trajectories are all unbounded in  $y$  and leave the jet region at smaller and smaller  $x$  as  $B_g$  increases.

In order to study jets and diffusion regions at *later* times we have performed additional implicit PIC reconnection simulations with a mass ratio of  $M/m = 256$  in a much larger simulation box of size  $200d_i \times 30d_i$ . Time histories of the reconnection rate ( $\propto -E_z(t)$ ) at the  $x$  point are shown in Fig. 5(a), together with  $v_{ex}/v_{\text{eth0}}$  at a late time.

For  $B_g = 0$  [Fig. 5(b)] the jets are well collimated and undeflected for as long as the simulation is run ( $t\Omega_i = 48$ ). Well-collimated jets are seen [Fig. 5(b)] emanating from the  $x$  line. For  $B_g = 0.1B_0$  the jets are deflected throughout the simulation, including at the late time  $t\Omega_i = 28$  [Fig. 5(c)] when the reconnection rate has plateaued.

Using an even lower mass ratio  $M/m = 25$ , we find that the jets are only slightly deflected for guide fields as large as  $B_g = 0.2B_0$ . Therefore, the actual deflection of jets by small guide fields may be underestimated for unphysically small mass ratios.

Just as has been found in standard models of 2D MHD [4], a number of features of magnetic reconnection found in standard antiparallel 2D *kinetic* simulations are not robust enough to survive even very small modifications to the initial conditions. New implicit 2D PIC simulations

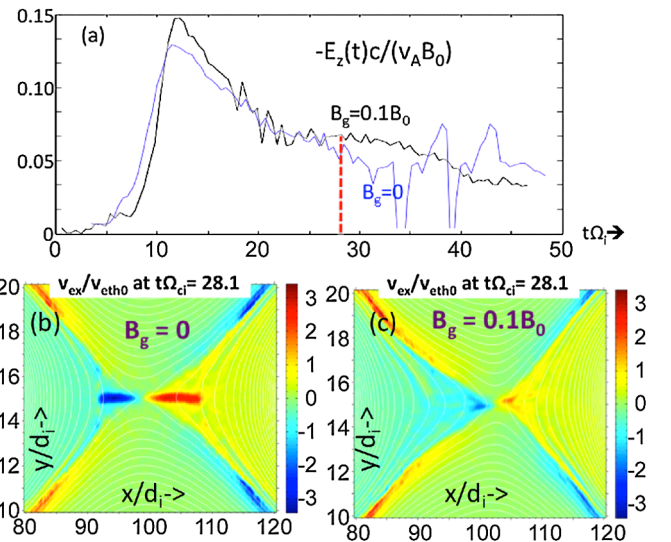


FIG. 5 (color online).  $M/m = 256$ . (a): Reconnection rate,  $-E_z(t)$ , (inflow drift)/(inflow Alfvén speed) near the  $x$  point for  $B_g = 0, 0.1B_0$ . (b), (c):  $v_{ex}(x, y)/v_{\text{eth0}}$  at time  $t\Omega_i = 28.1$  for  $B_g = 0, 0.1B_0$ .

of reconnection have revealed that surprisingly small guide fields can distort and deflect the collimated electron jets in  $v_{ex}$  found in PIC simulations initiated with a standard antiparallel geometry, in which there is no guide field. For a physical mass ratio of  $M/m = 1836$ , a guide field,  $B_g$ , as small as one-twentieth of the asymptotic reversing field in the initial Harris equilibrium,  $B_0$ , is sufficient to deflect early-forming jets. A dynamical treatment of electron dynamics very close to the  $x$  point during small guide field reconnection in a hydrogen plasma reveals the mechanism by which the Lorentz force of the guide field produces jet deflection for small guide fields. Early jet disruption by a guide field  $B_g = 0.1B_0$  can be sustained over long times, after the reconnection rate has begun to flatten, according to additional simulations with  $M/m = 256$ . The reconnection rate is essentially unchanged with the addition of such a small guide field, even though the narrow well-collimated “outer diffusion regions” of standard *antiparallel* reconnection simulations is destroyed along with the jets.

However, weak guide-field jet deflection found in these new simulations is at odds with the interpretation of recent measurements as undeflected electron jets along  $x$  in the presence of a weak guide field (Fig. 1). A resolution of this discrepancy may be possible through a reinterpretation of the observations. For example, the geometry of the reconnection exhaust depicted in Ref. [7], Fig. 2, could be generalized to allow for a deflected jet. Alternatively, this discrepancy *may* suggest shortcomings in modeling reconnection in the magnetosheath using widely accepted simulation approximations. Preliminary studies show that the colder electron temperatures in the sheath are probably not responsible for the discrepancy. Jet deflection also appears to persist in 3D PIC simulations.

Whatever the resolution, almost all real reconnection events involve small guide fields and their effect on

electron jets and on other features of reconnection need to be understood. Measurement of such electron features of magnetic reconnection will be one of the main thrusts of the upcoming NASA Magnetospheric Multiscale (MMS) mission and kinetic simulations must become more realistic in order to interpret such measurements physically.

This work was supported by NASA MMS Grant No. NNX08AO84G. We wish to thank Jan Egedal, Tai Phan, Forest Mozer, and Michael Shay for useful discussions.

- 
- [1] M. A. Shay, J. F. Drake, and M. Swisdak, *Phys. Rev. Lett.* **99**, 155002 (2007).
  - [2] H. Karimabadi *et al.*, *Geophys. Res. Lett.* **34**, L13104 (2007).
  - [3] K. Fujimoto, *Phys. Plasmas* **13**, 072904 (2006).
  - [4] W. H. Matthaeus and S. L. Lamkin, *Phys. Fluids* **28**, 303 (1985); *Phys. Fluids* **29**, 2513 (1986); W. Wan and G. Lapenta, *Phys. Rev. Lett.* **101**, 015001 (2008); P. Dmitruk and W. H. Matthaeus, *Phys. Plasmas* **13**, 042307 (2006); S. Servidio *et al.*, *Phys. Rev. Lett.* **102**, 115003 (2009).
  - [5] Swisdak *et al.*, *J. Geophys. Res.* **110**, A05210 (2005); Karimabadi *et al.*, *J. Geophys. Res.* **110**, A03213 (2005).
  - [6] G. Lapenta *et al.*, *Phys. Plasmas* **17**, 082106 (2010); S. Markidis *et al.*, *Math. Comput. Simul.* **80**, 1509 (2010).
  - [7] T. D. Phan *et al.*, *Phys. Rev. Lett.* **99**, 255002 (2007).
  - [8] Hesse *et al.*, *Phys. Plasmas* **6**, 1781 (1999).
  - [9] A. Le *et al.*, *Phys. Plasmas* **17**, 055703 (2010); *Geophys. Res. Lett.* **37**, L03106 (2010).
  - [10] T. W. Speiser, *J. Geophys. Res.* **70**, 4219 (1965).
  - [11] Trajectories with many different initial conditions were studied both analytically and numerically, using forces from simulations. All were found to accelerate in  $x$  and oscillate in  $y$  as found for this characteristic trajectory.